Heliyon 10 (2024) e29309

Contents lists available at ScienceDirect

Heliyon

journal homepage: www.cell.com/heliyon

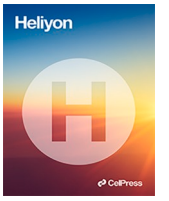

Research article

Assessment of thermohydraulic performance and entropy generation in an evacuated tube solar collector employing pure water and nanofluids as working fluids

Oscar A. López-Núñez [a,*], F. Lara [a], A. González-Angeles [a], A. Cardenas-Robles [a], J.J. Ramírez-Minguela [b], J. Arturo Alfaro-Ayala [b]

[a] Facultad de Ingeniería, Universidad Autónoma de Baja California, Blvd. Benito Juárez s/n, C.P. 21280, Mexicali, Baja California, Mexico
[b] Department of Chemical Engineering, University of Guanajuato, DCNE, Col. Noria Alta s/n, C.P. 36050, Guanajuato, Gto, Mexico

ARTICLE INFO

Keywords:
TiO_2 nanofluid
Entropy generation
Numerical model
Computational fluid dynamics

ABSTRACT

This study conducts a numerical comparison of the thermal performance of three distinct working fluids (pure water, TiO_2, and SiO_2 water-based nanofluids) within an evacuated tube solar collector using Computational Fluid Dynamics. The study evaluates thermohydraulic performance alongside global and local entropy generation rates, while considering variations in solar radiation values and inlet mass flow rates. Results indicate that nanofluids demonstrate superior performance under low solar radiation, exhibiting higher outlet temperatures, velocities, thermal efficiency, and exergy efficiency compared to pure water. However, at the higher solar radiation level, the efficiency of SiO_2 water-based nanofluid diminishes due to its impact on specific heat. Furthermore, the entropy generation analysis reveals significant reductions with TiO_2 water-based nanofluid in all the phenomena considered (up to 79 %). The SiO_2 nanofluid performance aligns closely with pure water under high radiation value. This investigation offers valuable insights into the utilization of nanofluids in solar collectors across diverse operating conditions, emphasizing their pivotal role in enhancing overall performance.

1. Introduction

The solar energy has been a renewable and freely available resource, which plays a pivotal role in mitigating the escalating environmental pollution associated with fossil fuel consumption, particularly in developing nations [1,2]. Its inherent friendly compatibility, high efficiency, and capacity to meet sustainability and quality energy demands surpasses that of various alternative renewable energy sources [3].

The devices that can harvesting the solar energy potential in a low temperature application (less than 100 °C) are called solar collectors. In this sense, the evacuated tube solar collector (ETSC) transforms the solar energy into heat energy by a series of parallel concentric glass tubes that are connected to a manifold. The vacuum insulation between the concentric tubes allows to minimize the heat losses of the fluid inside the collector (called working fluid), which absorbs the heat from the solar radiation. The ETSCs have been in increasing demand in widespread industrial applications, serving as a sustainable and renewable energy source for various purposes, such as drying, sterilization, distillation, and desalination, among others.

* Corresponding author.
E-mail address: oscar.lopez.nunez@uabc.edu.mx (O.A. López-Núñez).

https://doi.org/10.1016/j.heliyon.2024.e29309
Received 12 January 2024; Received in revised form 3 April 2024; Accepted 4 April 2024
Available online 5 April 2024

Nomenclature

A_c	Surface area (m^2)
c	Specific heat (J kg^{-1} K^{-1})
D^*	Normalized diameter
$\dot{E}_{solar}$	Exergy production of the solar irradiation (W)
$\dot{E}_{useful}$	Useful exergy production (W)
$\vec{g}$	Gravity (m s^{-2})
I	Incident solar radiation (W m^{-2})
k	Thermal conductivity (W m^{-1} K^{-1})
$\dot{m}$	Inlet mass flow rate (Kg s^{-1})
P	Pressure (Pa)
$\dot{Q}_{in}$	Solar energy gain rate (W)
$\dot{Q}_{loss}$	Heat loss (W)
$\dot{Q}_{useful}$	Useful heat (W)
s	Local form of entropy generation rate (W $m^{-3}K^{-1}$)
S_i	Global form of entropy generation rate for each phenomenon (W K^{-1})
S_t	Total entropy generation rate (W K^{-1})
T	Temperature (°C)
T_{env}	Environmental temperature (°C)
T_{in}	Inlet temperature (°C)
T_{out}	Outlet temperature (°C)
T_{sun}	Solar intensity temperature (K)
$\vec{u}$	Velocity (m s^{-1})

Subscripts

bf	Base fluid
v	Entropy generation rate attributed to viscous effects
nf	Nanofluid
np	Nanoparticle
h	Entropy generation rate attributed to heat transfer
w	Water

Greek letters

δ	Regression coefficient
η	Thermal efficiency
η_e	Exergy efficiency
μ	Dynamic viscosity (Pa s)
ρ	Density (kg m^{-3})
φ	Nanoparticle Concentration (% vol)
χ	Property of the nanofluid in the temperature polynomials

Abbreviation

CFD	Computational Fluid Dynamics
CV	Computed Values
ETSC	Evacuated Tube Solar Collector
GV	Guess Values
UDF	User-Defined Function

In recent times, there has been a growing interest in investigating the use of nanofluids as enhanced working fluids to increase the performance of diverse heat transfer devices, including solar technologies such as ETSCs [4,5]. Nanofluids, comprised of nanoparticles typically smaller than 100 nm dispersed within a base fluid (usually water), possess distinct thermal properties compared to the base fluid alone. This mixture serves as a more thermally efficient working fluid, augmenting thermal conductivity while diminishing specific heat capacity. Consequently, nanofluids offer improved overall fluid performance in comparison to pure working fluids. Therefore, the integration of nanofluids as working fluids enhances the performance of an ETSC [6,7]. Mahendran et al. [8] experimentally determined the outlet temperature and efficiency of an ETSC using TiO_2 water-based nanofluid. The results indicated an increment of 19 % and 16.6 % in the outlet temperature and thermal efficiency, respectively, in comparison to using pure water as a working fluid. Kim et al. [9] conducted a theoretical investigation using different water-based nanofluids in an ETSC. Their study observed an increase in thermal efficiency, ranked from highest to lowest as follows: CuO, Al_2O_3, TiO_2 and SiO_2. Additionally, they

noted the potential for reducing the annual amount of greenhouse gases by employing multiple solar collectors simultaneously. Daghigh and Zandi [10] performed an experimental arrangement to investigate an ETSC comparing CuO and TiO_2 water-based nanofluids. It was found that the collector's efficiency improved by 12 % and 5 % respectively in comparison with pure water as the working fluid. Elshazly et al. [11] evaluated the use of Al_2O_3 water-based nanofluid as the working fluid in an ETSC. Their experimental results indicated a 12 % enhancement in efficiency compared to using pure water. Hosseini and Shafiey [12] carried out an experimental investigation on the use of TiO_2 water-based nanofluid in an ETSC. They reported an increase in thermal conductivity as well as an enhancement of the collector efficiency by up to 12.2 %. Sasikumar et al. [13] performed an experimental study on parallel type ETSC using Al_2O_3 water-based nanofluid. The results revealed that the maximum outlet temperature and thermal efficiency was achieved at the highest particle concentration (0.3 %).

While the previous studies have primarily centered on experimental investigations of ETSCs, conducting such experiments requires specialized equipment, which can be prohibitively expensive. Consequently, Computational Fluid Dynamics (CFD) has emerged as a cost-effective alternative for analyzing the use of nanofluids as working fluids in ETSCs. Yan et al. [14] presented a numerical and experimental investigation to assess the impact of SiO_2 nanofluid as the working fluid in an ETSC. The results demonstrated an increase in the velocity of the working fluid, along with a rise in the temperature of the fluid inside the tubes, reaching up to 9.7 °C. Mercan and Yurddas [15] developed a CFD model of an ETSC to examine the influence of different parameters on the collector's performance, including the type of nanofluid, collector tilt angle, and the number of evacuated tubes. Their findings indicated a significant enhancement in the outlet temperature when the collector was inclined at a 30° angle with 36 tubes. Also, it was observed a 3.93 % increase in the outlet temperature for Al_2O_3 nanofluid and a 6.63 % increase for CuO nanofluid. In this sense, Yurddas [16] conducted a CFD study using various water-based nanofluids within an ETSC configuration inclined at a 30° angle. The results showed that the outlet temperature improved by 3.25 %, 6.24 % and 14.09 % using SiO_2, TiO_2, and Cu water-based nanofluids respectively. Hasan et al. [17] conducted a numerical investigation on a solar thermal collector using SiO_2 water-based nanofluid at different nanoparticle concentrations. The CFD model showed that a 5 % concentration of the nanofluid resulted in the highest Nusselt number. Tabarhoseini and Sheikholeslami [18] introduced a CFD numerical model focusing on a section of an ETSC employing Cu water-based nanofluid. The analysis examined the temperature distribution along the absorber tube, revealing that the utilization of nanofluids led to increased average manifold temperature and enhanced thermal efficiency.

Previous studies have focused on analyzing the thermal performance of the ETSC. However, quantifying and identifying internal system irreversibilities are crucial steps necessary to enhance the performance of the ETSC. The entropy generation rate analysis serves as a valuable metric for assessing the magnitude of irreversibilities arising from different phenomena [19,20]. Lower entropy generation rate indicates fewer irreversible losses, allowing the solar collector to effectively harness and utilize solar energy for heat generation. To the best of the authors' knowledge, there is a limited literature dedicated to quantifying and characterizing entropy generation in an ETSC employing nanofluid as the working fluid. Gan et al. [21] evaluated the performance and global entropy generation in an ETSC using TiO_2 nanofluid. Their results showed a 16.5 % improvement in thermal efficiency and a 1.23 % decrease in the entropy generation rate, attributed to the high thermal conductivity of the nanofluid. More recently, Kumar and Tiwari [22] assessed the thermal performance and global entropy generation rate in an ETSC utilizing boron nitride (BN) water-based nanofluid at various concentrations. Their results indicated that the highest thermal efficiency was achieved at a concentration of 1.5 %, while the lowest entropy generation rate was observed at a concentration of 1.25 %. Nevertheless, the global formulation of the entropy generation leads to ignoring the specific location of the irreversibilities. In this sense, Tabarhoseini and Sheikholeslami [23] developed a CFD model for an ETSC employing CuO nanofluid as the working fluid. Their analysis encompassed the assessment of entropy generation rate in both global and local forms, considering various phenomena. Their findings not only identified the precise locations of irreversibilities but also demonstrated a reduction in entropy generation through the use of nanofluid. However, the numerical model only considers a simplified solar collector geometry, incorporating a single solar radiation value and using only one type of nanofluid. Consequently, accurately predicting the performance of the ETSCs remains a challenging task.

Given the absence of comparative studies exploring the utilization of nanofluids as working fluids in a complete ETSCs and the limited analysis conducted under varied operating conditions, this study endeavors to address this gap in the literature. The present study is dedicated to comparing the thermohydraulic and entropy performance of an ETSC utilizing TiO_2 and SiO_2 water-based nanofluids, as well as pure water. TiO_2 and SiO_2 water-based nanofluids are selected for their widespread use in previous research and also due to their potential to enhance the thermal properties of the working fluid [24,25]. The simulations considered a complete ETSC geometry as well as variations in solar radiation and mass flow rate. Furthermore, a comparative analysis of both local and global entropy generation rate was conducted, considering the influence of viscous effects, heat transfer, and heat losses. Given the increasing importance of harnessing solar energy for mitigating environmental impacts and meeting energy demands, this comparative study contributes to the advancement of solar thermal technology.

2. Geometry and mathematical models

The geometry of the evacuated tube solar collector (ETSC) is based in Ramírez-Minguela et al. [26]. It consists of 36 evacuated tubes linked to a manifold with each tube measuring 1.5 m in length. The evacuated tubes have internal and external diameters of 0.047 and 0.058 m, respectively. The manifold has a length of 2.50 m with an internal diameter of 0.130 m, and the surface area (A_c) is 3.14 m^2 (Fig. 1). Based on the above dimensions, a 3D geometry was constructed through the commercial software ANSYS-Fluent®.

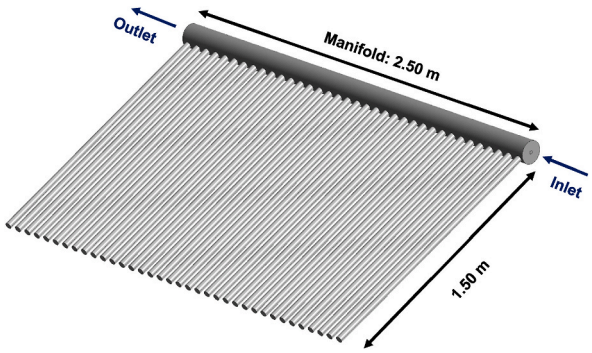

Fig. 1. 3D Geometry used for the ETSC.

2.1. Governing equations

The behavior of the working fluids in the ETSC is governed by the continuity, momentum, and energy equations. These equations are solved using the commercial software ANSYS-Fluent® under the following assumptions [27,28].

- Steady state conditions.
- Laminar flow.
- Properties depending on the temperature of the working fluids.

Specifically, the three-dimensional continuity, momentum and energy equations are expressed as follows in Eqs. (1)–(3) [29,30]:

$$\text{Continuity}: \nabla \bullet (\rho \bullet \vec{\boldsymbol{u}}) = 0 \tag{1}$$

$$\text{Momentum}: \nabla \bullet (\rho \bullet \vec{\boldsymbol{u}} \bullet \vec{\boldsymbol{u}}) = -\nabla P + \nabla \bullet (\mu \nabla \vec{\boldsymbol{u}}) + \rho \vec{\boldsymbol{g}} \tag{2}$$

$$\text{Energy}: \nabla \bullet (\rho \vec{\boldsymbol{u}} cT - k\nabla T) + \nabla \bullet q_R = 0 \tag{3}$$

Where "$\bullet$" refers to the element-wise (Hadamard) product and the source term $\nabla \bullet q_R$ represents the radiation intensity entering the tubes of the solar collector. This is determined by the solar load model solution, which is incorporated within the ANSYS-Fluent® software. The use of this model is common in simulating solar thermal devices and has been applied in previous studies [31].

On the other hand, the thermal efficiency of the ETSC using different working fluids is computed as follows in equation (4) [32]:

$$\eta = \frac{\dot{Q}_{useful}}{\dot{Q}_{in}} = \frac{\dot{m}c(T_{out} - T_{in})}{A_c I} \tag{4}$$

where $\dot{Q}_{useful}$ and $\dot{Q}_{in}$ represent the useful heat and the rate of solar energy gain, respectively.

The exergy efficiency is determined by the following equation (5) [33]:

$$\eta_e = \frac{\dot{E}_{useful}}{\dot{E}_{solar}} \tag{5}$$

The calculation of the useful exergy production ($\dot{E}_{useful}$) is done by equation (6) as [34]:

$$\dot{E}_{useful} = \dot{m}c\left[T_{out} - T_{in} - T_{env}\ln\left(\frac{T_{out}}{T_{in}}\right)\right] \tag{6}$$

The expression for the exergy production of the solar irradiation ($\dot{E}_{solar}$) is defined by equation (7) as [35]:

$$\dot{E}_{solar} = A_c I\left[1 + \frac{1}{3}\left(\frac{T_{env}}{T_{sun}}\right)^4 - \frac{4}{3}\left(\frac{T_{env}}{T_{sun}}\right)\right] \tag{7}$$

where T_{sun} represents the solar intensity temperature and is considered as 5770 K [36].

2.2. Pure water and water-based nanofluids properties

The properties of the working fluids (water, TiO_2 and SiO_2 water-based nanofluids) such as density (ρ), thermal conductivity (k), specific heat (c) and viscosity (μ), were modeled using temperature polynomials to account for buoyancy effects. These temperature polynomials are valid within the temperature range of 5 °C–95 °C.

For water, the polynomials are provided in Eqs. (8)–(11) [37].

$$\rho_w = 1001 - 0.0834T - 0.0035T^2 \tag{8}$$

$$k_w = 0.5634 + 0.002T - 8 \times 10^{-6}T^2 \tag{9}$$

$$c_w = 4215 - 2.3787T + 0.0528T^2 - 0.0005T^3 + 2 \times 10^{-6}T^4 \tag{10}$$

$$\mu_w = 0.0017 - 5 \times 10^{-5}T + 9 \times 10^{-7}T^2 - 8 \times 10^{-9}T^3 + 3 \times 10^{-11}T^4 \tag{11}$$

On the other hand, the polynomials of the nanofluids are based on the estimation of their properties at a fixed temperature given by Eqs. (12)–(15) [38–40].

$$\rho_{nf} = (1-\varphi)\rho_{bf} + \varphi\rho_{np} \tag{12}$$

$$k_{nf} = k_{bf}\left(\frac{k_{np} + 2k_{bf} + 2\varphi(k_{np} - k_{bf})}{k_{np} + 2k_{bf} - \varphi(k_{np} - k_{bf})}\right) \tag{13}$$

$$c_{nf} = \frac{(1-\varphi)c_{bf}\rho_{bf} + \varphi c_{np}\rho_{np}}{\rho_{nf}} \tag{14}$$

$$\mu_{nf} = \mu_{bf}\left(1 + 5\varphi + 80\varphi^2 + 160\varphi^3\right) \tag{15}$$

The properties for the nanofluid, base fluid (pure water), and nanoparticle are represented by the subscripts *"nf", "bf"* and *"np"*, respectively.

The properties of the nanoparticles used (TiO_2 and SiO_2), are presented in Table 1.

By combining Eqs. (8)–(15) and using the properties of the nanoparticles outlined in Table 1, the temperature polynomials for the nanofluids (TiO_2 and SiO_2) are derived and presented as follows (Equation (16)) [44]:

$$\chi = \sum_{i=0} \delta_i T^i \tag{16}$$

Where χ represents a property of the fluid, while δ_i stands for the regression coefficient. These coefficients are provided in Table 2 for both nanofluids.

Table 1
Properties of the TiO_2 and SiO_2 nanoparticles used for the analysis.

Property	TiO_2 Value [41,42]	SiO_2 Value [43]
Density, ρ_{np} (kg/m^3)	4260	2400
Thermal Conductivity, k_{np}, (W/mK)	8.4	1.4
Specific Heat, c_{np}, (J/KgK)	692	745
Particle Size (nm)	21	30
Nanoparticle Concentration, φ, (% vol)	0.5	0.5

Table 2
Coefficients used in the temperature polynomials of the nanofluids.

	ρ_{TiO_2}	ρ_{SiO_2}	k_{TiO_2}	k_{SiO_2}	c_{TiO_2}	c_{SiO_2}	μ_{TiO_2}	μ_{SiO_2}
δ_0	786.68	850.41	− 0.7924	− 0.8961	546235.05	491612.10	0.4207	0.4652
δ_1	1.78	1.70	0.0076707	0.0086943	− 8362.11	− 7528.57	$-4.8514x10^{-3}$	$-5.3647x10^{-3}$
δ_2	− 0.003423	− 0.003272	$-1.004x10^{-5}$	$-1.138x10^{-5}$	51.48	46.37	$2.1102x10^{-5}$	$2.3336x10^{-5}$
δ_3	–	–	–	–	− 0.1581	− 0.1425	$-4.095x10^{-8}$	$-4.528x10^{-8}$
δ_4	–	–	–	–	$2.42x10^{-4}$	$2.18x10^{-4}$	$3x10^{-11}$	$3.3x10^{-11}$
δ_5	–	–	–	–	$-1.48x10^{-7}$	$-1.33x10^{-7}$	–	–

2.3. Formulation of local and global entropy generation rate

The local entropy generation rate results from the phenomena of viscous effects (s_v) and heat transfer (s_h) taking place within the working fluids (water or water-based nanofluids). Each contribution is obtained by an infinitesimal volume balance and is expressed by Eqs. (17) and (18) as [45]:

$$s_v = \frac{\mu}{T}\left\{2\left[\left(\frac{\partial u_x}{\partial x}\right)^2 + \left(\frac{\partial u_y}{\partial y}\right)^2 + \left(\frac{\partial u_z}{\partial z}\right)^2\right] + \left(\frac{\partial u_x}{\partial y} + \frac{\partial u_y}{\partial x}\right)^2 + \left(\frac{\partial u_x}{\partial z} + \frac{\partial u_z}{\partial x}\right)^2 + \left(\frac{\partial u_y}{\partial z} + \frac{\partial u_z}{\partial y}\right)^2\right\} \tag{17}$$

$$s_h = \frac{k}{T^2}\left[\left(\frac{\partial T}{\partial x}\right)^2 + \left(\frac{\partial T}{\partial y}\right)^2 + \left(\frac{\partial T}{\partial z}\right)^2\right] \tag{18}$$

On the other hand, each contribution to the global entropy generation rate is determined by integrating it throughout the entire volume of the solar collector (Equation (19)) [46].

$$S_i = \int s_i dV \tag{19}$$

for $i = \{v, h\}$. Furthermore, the entropy generation rate attributed to heat loss is taken into account by equation (20) [26]:

$$S_q = \frac{\dot{m}c(T_{out} - T_{in}) - A_c I}{T_{env}} \tag{20}$$

$\dot{Q}_{loss}$ stands for the heat loss and T_{env} represents the environmental temperature. Finally, the total entropy generation rate is calculated by summing all the global contributions (expressed in equation (21)):

$$S_t = S_i + S_q \tag{21}$$

2.4. Boundary and operating conditions

The following boundary conditions were employed in the CFD model: a specified mass flow rate at the inlet of the working fluid (20 °C) and atmospheric pressure at the exit of the ETSC. Solid surfaces, including tubes and manifold, were designated as walls, and convective heat transfer from the surroundings of the ETSC was also taken into account.

The properties of the tubes, such as density, thermal conductivity and specific heat are: 2230 kg/m^3, 1.2 W/(m)(K), and 800 J/(Kg)(K), respectively. Also, the optical properties such absorbance and transmittance are 0.92 and 0.95 respectively. More information about the properties used in the numerical model can be found in Ref. [37].

The simulations took into account the variations in operating conditions, including changes in the working fluid, solar radiation and inlet mass flow rate. Two solar radiation values were considered (735 and 935 W/m^2) along with four different inlet mass flow rate values [47,48]. Purified water, along with SiO_2 and TiO_2 nanofluids served as the working fluids.

A total of 24 simulations were conducted, combining the specified operating conditions. Fig. 2 summarizes the operating conditions for the CFD simulations.

2.5. Solution procedure

To acquire the distributions of the velocity and temperature, the SIMPLE algorithm was employed to solve the momentum and energy equations through the finite volume method. This numerical method ensures accurate conservation of the governing equations facilitating precise numerical simulations of fluid flow and heat transfer phenomena. Its flexibility in handling complex geometries and

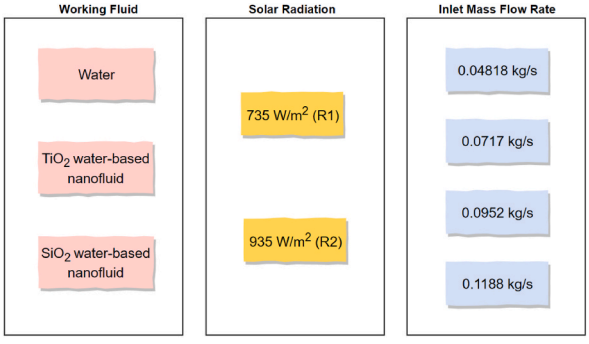

Fig. 2. Summary of the operating conditions used in the analysis.

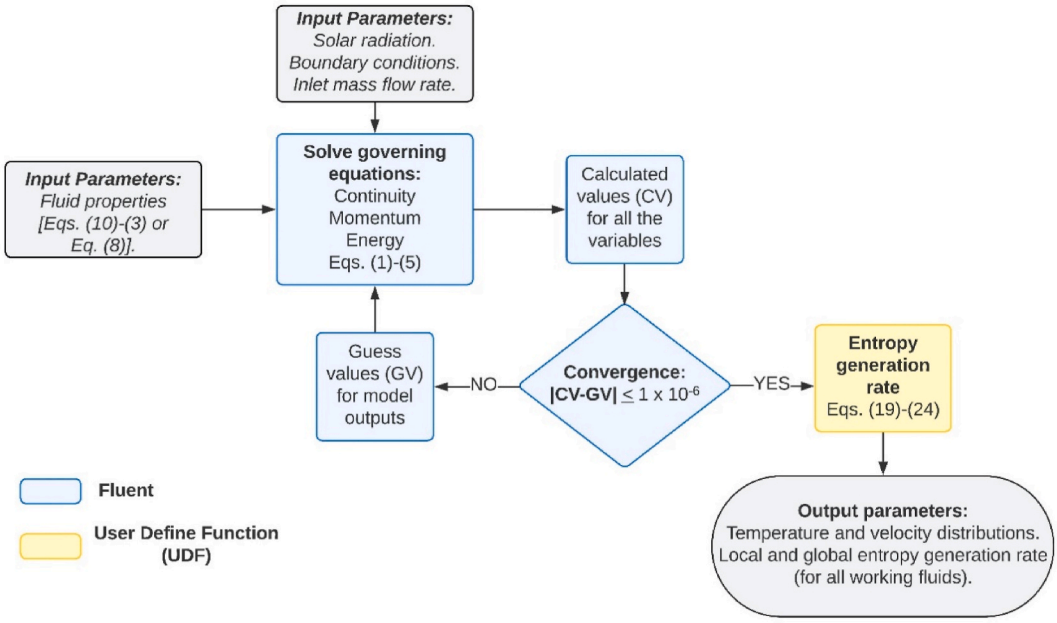

Fig. 3. Flowchart outlining the numerical modeling process for the ETSC.

conservation principles makes it an invaluable tool for understanding these types of applications. Fig. 3 presents the general solution procedure of the simulation for the ETSC. The initial estimates, referred to as Guess Values (GV), serve as the initial values for the iterative process. During each iterative step, the GVs are substituted with newly computed values (CV) until the convergence criterion of $1.0\,x\,10^{-6}$ is met. A user-defined function (UDF) was used as a post-processing step to calculate the entropy generation rate.

2.6. Mesh analysis

A mesh independence analysis was conducted to optimize computational efficiency in calculating the thermohydraulic performance of the ETSC. Both tetrahedral and hexahedral elements ranging from 0.15 million to 6.4 million were taken into account. The simulations considered a solar radiation value of 935 W/m^2 (R2) with a mass flow rate of 0.04818 kg/s using TiO_2 nanofluid as the working fluid. The outlet temperature was monitored in each simulation and depicted in Fig. 4.

It is observed that for a mesh number higher than 1.02 million, the temperature exhibits independent behavior regardless of the mesh used. Therefore, the 24 simulations carried out in this study were conducted with 1.02 million elements. Finally, Fig. 5 shows the mesh used in the numerical model.

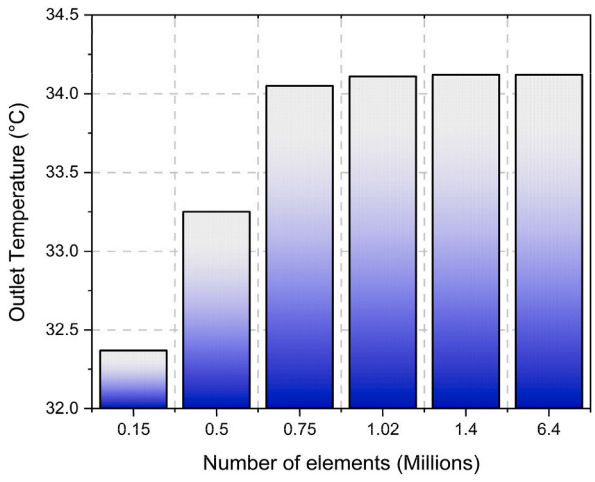

Fig. 4. Mesh independence analysis.

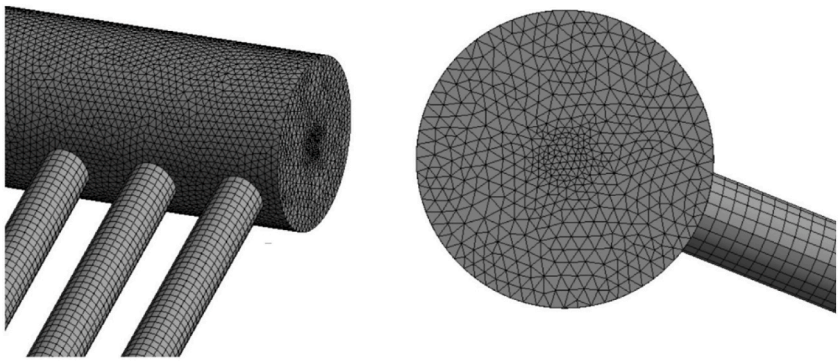

Fig. 5. Mesh used for the numerical model.

3. Findings and discussion

The following sections offer detailed insights into three key aspects: the validation of the polynomial equations, the validation of the numerical model, and the main findings derived from employing pure water, TiO_2 and SiO_2 nanofluids.

3.1. Validation of the polynomial equations for water-based nanofluids

A verification of the temperature polynomials for the nanofluids properties was conducted by comparing them with experimental data from the existing literature [49–51]. The same parameters of the nanoparticles used in the experimental setups were consistent with those employed in this study.

Fig. 6 shows the comparisons of density and thermal conductivity. Specifically, Fig. 6a illustrates the experimental and polynomial results for density. It is observed that the polynomials for both nanofluids exhibit trends that align with the experimental findings. To assess the difference between experimental and polynomial values, the root-mean square deviation (RMSD) index was obtained [52]. The RMSDs for the density of TiO_2 and SiO_2 water-based nanofluids were 0.44 % and 0.25 % respectively. These values indicate an acceptable level of accuracy for the density polynomial.

Fig. 6b demonstrates the juxtaposition of thermal conductivity between experimental and polynomial data. The polynomial for SiO_2 nanofluid exhibits a consistent trend with experimental findings. Moreover, the thermal conductivity polynomial of the TiO_2 water-based nanofluid has a less upward trend than the experimental results. However, the RMSD obtained for the TiO_2 water-based nanofluid was 1.73 %, while for the SiO_2 water-based nanofluid it was 0.72 %. Once again, these values indicate acceptable level of accuracy for the thermal conductivity polynomial.

Considering the outcomes, the temperature polynomials for nanofluid properties can be employed in numerical simulations of an ETSC.

It is noteworthy that the behavior of the nanofluid properties follows a similar trend to that of water. For instance, with increasing temperatures, there is a decline in density, but it is notable that the nanofluids exhibit higher density values compared to water. Additionally, nanofluids exhibit higher values for thermal conductivity, a minor increase in viscosity, and a notable reduction in specific heat.

3.2. Validation of the numerical model

To validate the numerical model, a comparison of the outlet temperature obtained through simulation was conducted against the results reported in the literature for the three working fluids [16,53]. It was ensured that the same operational conditions reported in the literature were used to ensure a fair comparison.

Table 3 presents the outlet temperature values alongside the corresponding relative error percentages for each working fluid. The analysis reveals relative errors of less than 3.3 % across all three working fluids. Furthermore, the highest relative error occurs with the nanofluids as working fluids. This is primarily attributed to the distinct ETSC geometry, which includes a heat exchanger inside the manifold. Nevertheless, due to the results obtained, the numerical model developed is capable of predicting the behavior of a solar device such as the ETSC.

3.3. Thermal-hydraulic performance

Fig. 7 illustrates the outlet temperature of the ETSC for each working fluid under different operating conditions. It is observed that the maximum outlet temperature is obtained with the highest solar radiation value of 935 W/m^2 (R2) at 0.04818 kg/s. When the TiO_2 nanofluid is using as the working fluid, there is an increase of 6.8 % and 6.5 % compared to pure water and SiO_2 nanofluid respectively. Moreover, the lowest outlet temperature is obtained at the solar radiation value of 735 W/m^2 (R1) with a mass flow rate of 0.1188 kg/s. A difference of 7.2 % is observed between TiO_2 nanofluid and pure water, and a difference of 4.3 % between both nanofluids. The

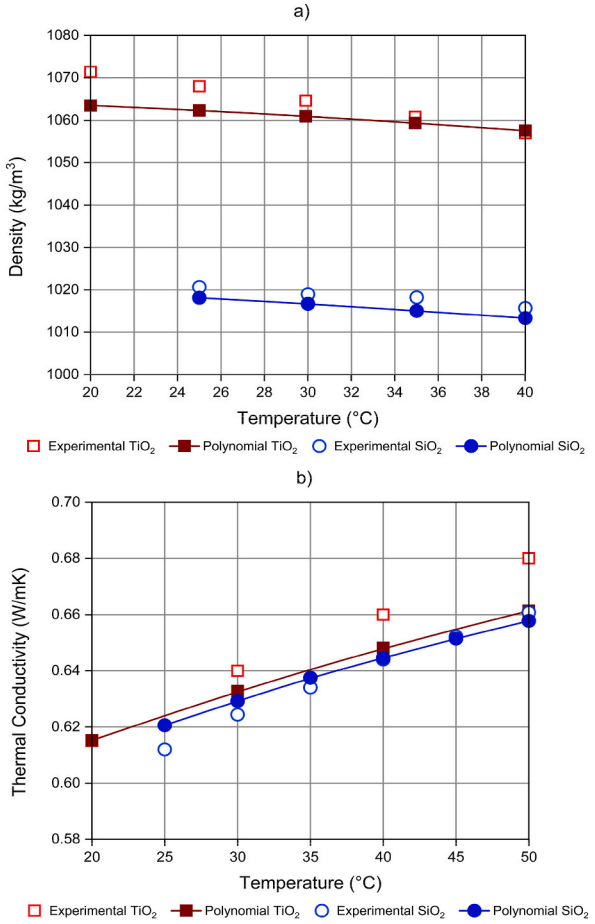

Fig. 6. Comparison of the water-based nanofluids polynomials against experimental results for: a) Density, and b) Thermal conductivity.

elevation in the outlet temperature is attributed to the higher thermal conductivity and lower specific heat obtained by the nanofluids. This combination enhances the heat transfer efficiency within the ETSC, leading to higher outlet temperatures compared to using purified water as the working fluid for all the cases.

Fig. 8 provides a comparative view of the temperature distribution throughout the entire ETSC when employing pure water (Fig. 8a), TiO_2 (Fig. 8b), and SiO_2 (Fig. 8c) nanofluids as working fluids. The contours were obtained under the solar radiation value of 935 W/m^2 using an inlet mass flow rate of 0.04818 kg/s.

A maximum temperature of 46.5 °C is obtained using pure water as working fluid, while using TiO_2 and SiO_2 water-based nanofluids, the maximum temperatures were around 37 °C and 35 °C respectively. However, it is noteworthy that employing pure water as the working fluid leads to minimum temperatures as low as 20 °C in several areas of the manifold and even within the evacuated tubes. This variation creates significant temperature gradients, ultimately resulting in lower average outlet temperatures. Consequently, the average outlet temperature is higher when nanofluids are utilized compared to using pure water, as illustrated previously in Fig. 7. Furthermore, the temperature distribution throughout the ETSC is influenced by the choice of working fluid, particularly evident when comparing pure water and nanofluids. The lower thermal diffusivity of the nanofluids promotes convective heat transfer, resulting in a more uniform temperature distribution. This phenomenon minimizes temperature gradients in areas prone

Table 3
Validation of the numerical model.

Working fluid	Outlet Temperature, T_{out} (°C)	% Relative error
Water	36.7 [53] 36.4	0.8
TiO_2 Nanofluid	38.46 [16] 37.3	3.1
SiO_2 Nanofluid	38.35 [16] 37.1	3.3

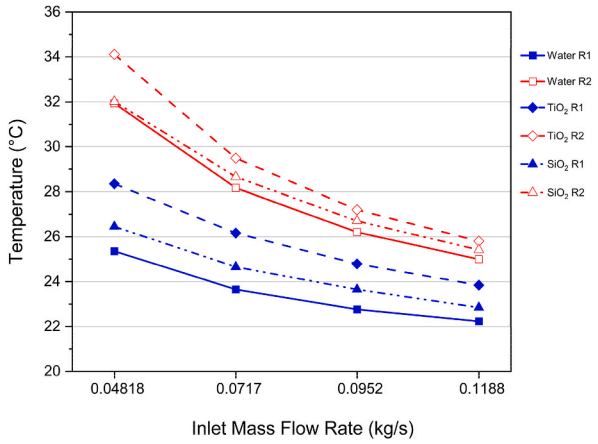

Fig. 7. Outlet temperature of the ETSC using nanofluids and pure water under various operating conditions.

to temperature fluctuations, such as within the manifold. Mathematically, it is observed that the local entropy generation rate due to heat transfer (Eq. (18)) is influenced by the temperature gradients within the system. Therefore, by reducing these temperature gradients and achieving a more homogeneous temperature distribution, the rate of entropy generation in the system decreases [54]. Finally, this behavior is attributed to the modifications in the properties of the base fluid induced by the nanoparticles (TiO_2 or SiO_2), particularly with regard to thermal conductivity and specific heat.

Fig. 9 presents a comparison of velocity profiles within the evacuated tubes of the ETSC for the three studied working fluids. Additionally, the comparison is conducted under a solar radiation value of 935 W/m^2 (R2) with an inlet mass flow rate of 0.04818 kg/s. The profiles were extracted along a vertical line representing a normalized diameter, D^*, ranging from 0 to 1, with 0.5 denoting the center of the tube. This line is positioned at the junction between the tube and the manifold. The profiles are shown for the initial tube (Fig. 9a), located at the inlet of the collector, the middle tube (Fig. 9b) and the final tube (Fig. 9c), located at the outlet of the collector.

In general, for all the working fluids, extremely low velocities inside the tubes were found. The positive values indicate fluid flow from the manifold, whereas negative values represent fluid flow returning to the manifold. The maximum velocity from the manifold to the tube is observed in the first and last tubes, reaching 15 mm/s when employing TiO_2 water-based nanofluid. On the other hand, the maximum velocity from the tube to the manifold is detected in all three ETSC tubes analyzed, approximately −25 mm/s, when using SiO_2 water-based nanofluid.

It is important to emphasize that, in all cases, higher velocities are achieved when nanofluids are employed as working fluids. This is attributed to the combined alterations in thermal properties. Furthermore, the SiO_2 water-based nanofluid presents higher density values than the TiO_2 water-based nanofluid, leading to lower kinematic viscosity values [55]. Because of this, the SiO_2 water-based nanofluid has higher velocity values among the three working fluids. However, the velocity values remain quite low for all the working fluids, leading to an exceedingly low entropy generation attributable to viscous effects.

The velocity profile maintains consistency across different operating conditions, aligning with patterns observed in varying solar radiation intensities and mass flow rate values (as stablished in section 2.4).

3.4. Thermal and exergy efficiency

Fig. 10 compares the thermal efficiency of purified water and nanofluids as working fluids, under varying solar radiation values (R1 and R2) and inlet mass flow rates. It is noted that for the lowest solar radiation value (R1), both nanofluids show higher thermal efficiency values than pure water across all the inlet mass flow rates. Furthermore, the TiO_2 nanofluid exhibits an average percentage increase of 24.5 % and 17.6 % compared to pure water and SiO_2 nanofluid, respectively, calculated by averaging the percentage increases across all mass flow rates values.

For the highest solar radiation value (R2), it is observed that employing SiO_2 nanofluid results in the lowest values of thermal efficiency among the three working fluids. However, its difference with respect to pure water decreases as the inlet mass flow rate increases. These low thermal efficiency values are due to a negative impact on the specific heat of the base fluid due to the SiO_2 nanoparticle [43]. Finally, the TiO_2 nanofluid has an average percentage increase of 6.9 % and 10.1 % in comparison with purified water and SiO_2 nanofluid respectively.

Fig. 11 compares the exergy efficiency of purified water and nanofluids under varying solar radiation values (R1 and R2) and inlet mass flow rates. It is noted that, for the lowest solar radiation value (R1), both nanofluids show higher exergy efficiency values across all inlet mass flow rates. Specifically, the TiO_2 nanofluid demonstrates an average percentage increase of 160 % and 78.4 % compared to using pure water and SiO_2 nanofluid respectively. These percentages are calculated by averaging the percentage increases across all mass flow rates values.

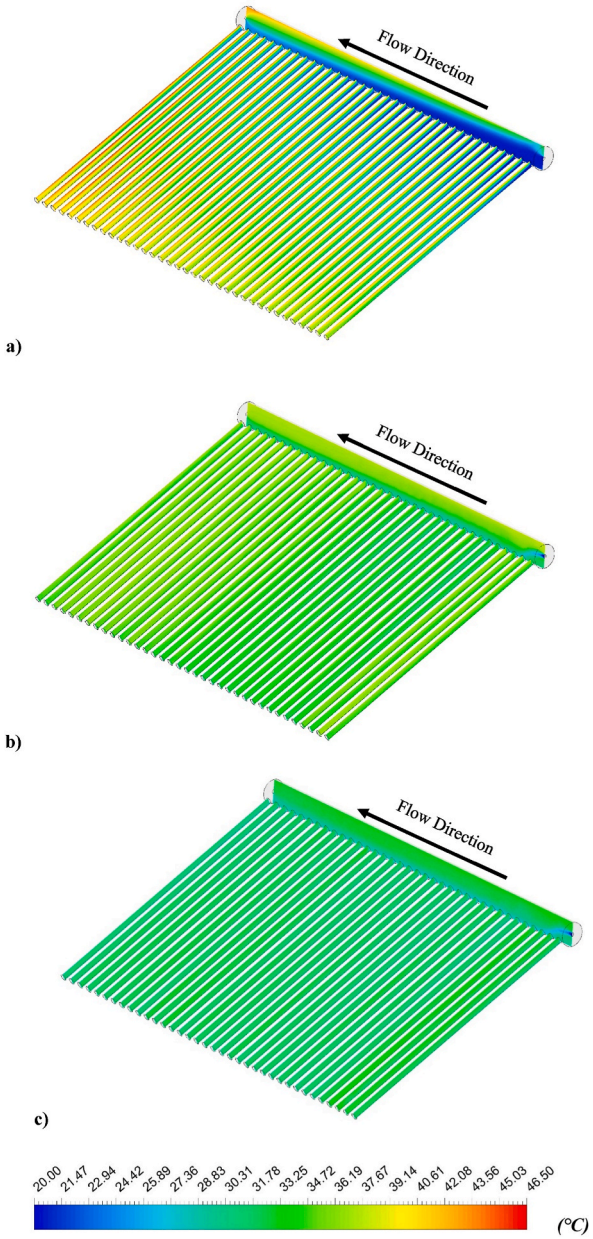

Fig. 8. Temperature distribution within the ETSC using a) Pure water b) TiO_2 nanofluid and c) SiO_2 nanofluid at 935 W/m^2 (R2) and an inlet mass flow rate of 0.04818 kg/s.

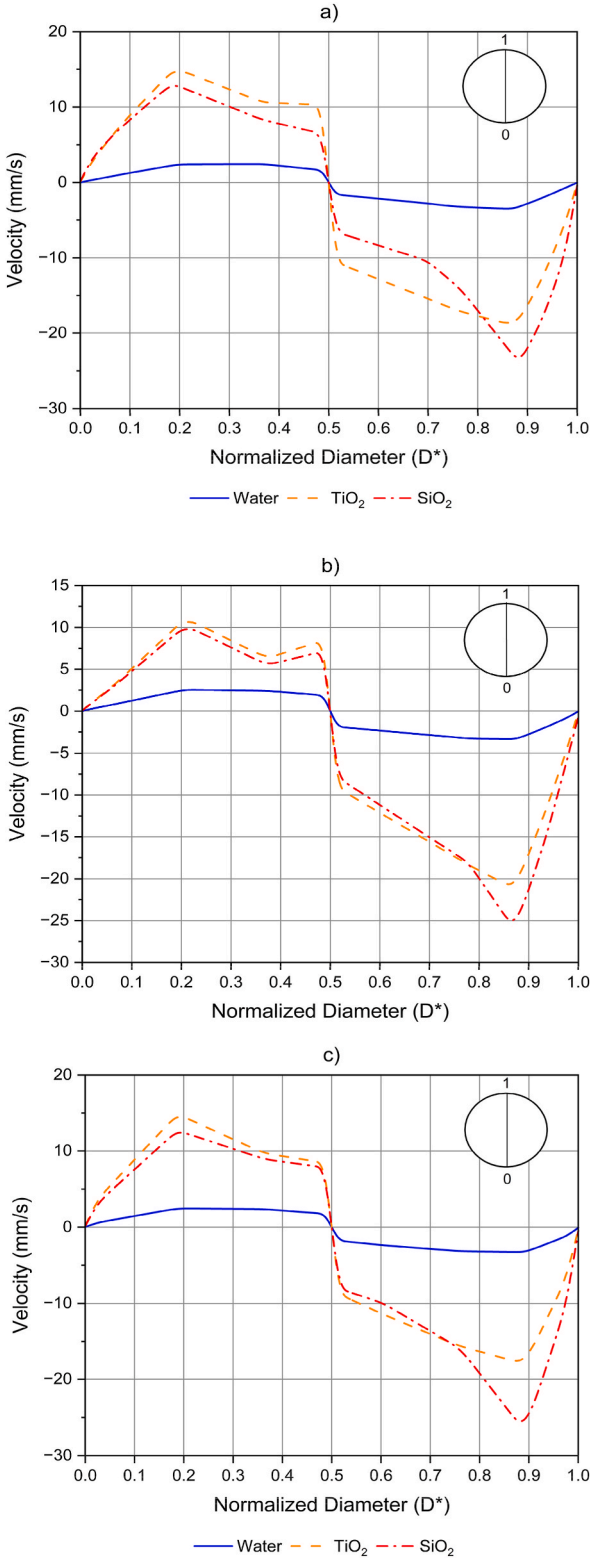

Fig. 9. Velocity profile distribution in: a) Initial tube, b) Middle tube, and c) Final tube of the evacuated tube solar collector at 935 W/m^2 (R2) and an inlet mass flow rate of 0.04818 kg/s.

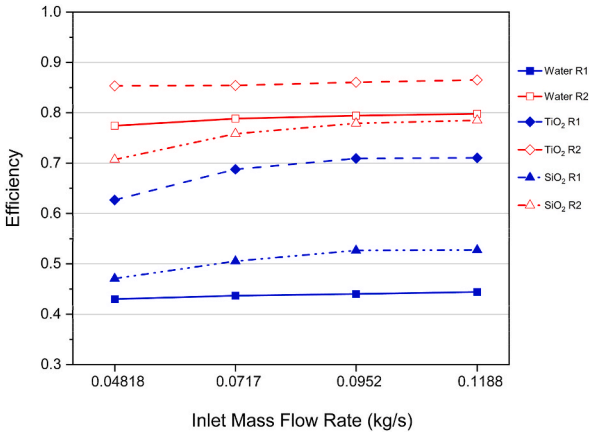

Fig. 10. Comparison of the thermal efficiencies of the ETSC using nanofluids and pure water under different operating conditions.

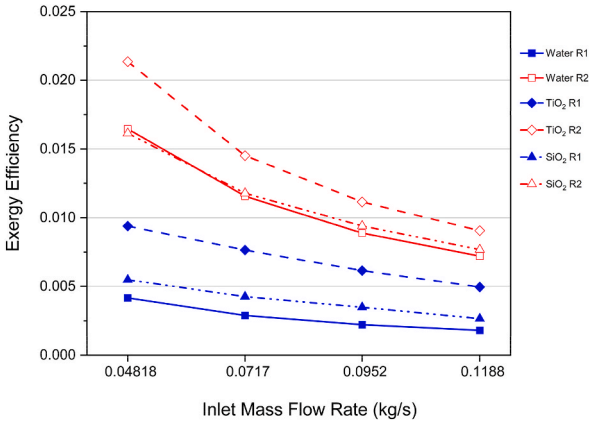

Fig. 11. Comparison of the exergy efficiencies of the ETSC using nanofluids and pure water under various operating conditions.

On the other hand, for the highest solar radiation value (R2) it can be noted that using SiO_2 nanofluid shows almost the same exergy efficiency values as pure water. Nevertheless, its difference increases as the inlet mass flow rate also increases. The TiO_2 nanofluid exhibits an average percentage increase of 26.6 % compared to using purified water and an 23 % increase compared to SiO_2 water-based nanofluid.

Finally, it is worth mentioning that the values obtained for the thermal and exergy efficiencies are in agreement with similar models reported in the literature [56,57].

3.5. Global form of the entropy generation rate

Fig. 12 provides a comprehensive assessment of the global entropy generation rate, considering variations in solar radiation values (735 W/m^2 and 935 W/m^2) while maintaining a constant inlet mass flow rate of 0.04818 kg/s.

The entropy generation rate attributed to viscous effects (S_v) exhibits extremely low values for both solar radiation levels and across all three working fluids (falling within the range of 10^{-6}). This minimal entropy generation rate is attributed to the exceptionally low velocity values observed within the ETSC, as depicted in Fig. 9. Thus, it can be inferred that the entropy generation rate caused by viscous effects is negligible in this particular solar collector design.

For the lowest solar radiation value (Fig. 12a), the entropy generation rate attributed to heat transfer (S_h) presents global values of 0.061 W/K, 0.014 W/K and 0.013 W/K for pure water, TiO_2 nanofluid and SiO_2 nanofluid respectively. This represents a decrease of 77.5 % between pure water and TiO_2 nanofluid, and 79 % between pure water and SiO_2 nanofluid. This reduction is related to the improvement in the temperature distribution (shown in Fig. 8). On the other hand, the global entropy generation rate attributed to heat loss (S_q) has values of 4.73 W/K for pure water, 2.67 W/K for TiO_2 water-based nanofluid and 4.38 W/K for SiO_2 nanofluid. This represents a reduction of 43.5 % between purified water and TiO_2 nanofluid and a 7.3 % decrease between purified water and SiO_2 nanofluid. This reduction is linked to the alterations in the specific heat of the nanofluids.

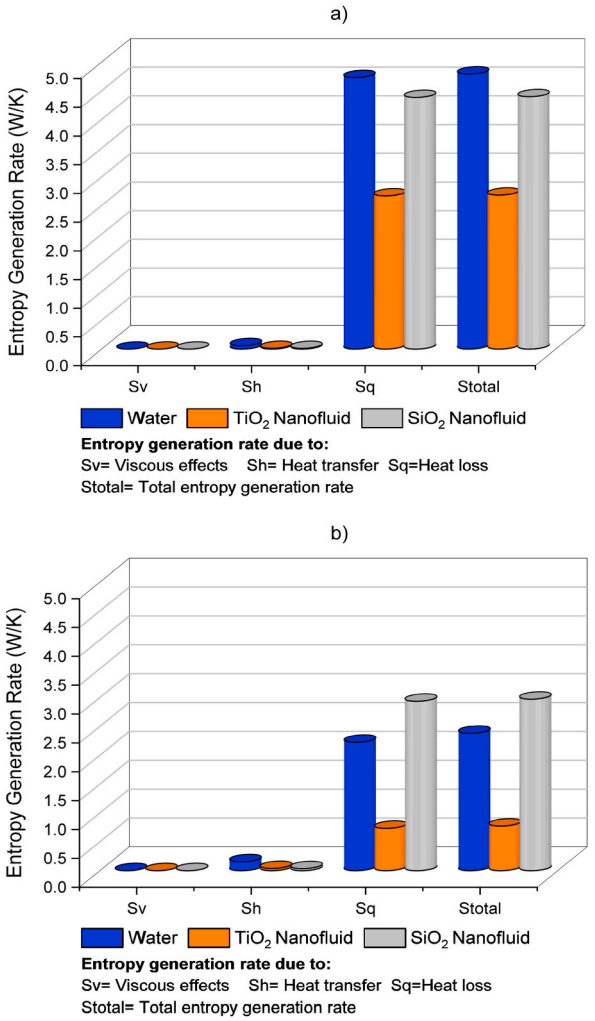

Fig. 12. Global form of the entropy generation rate with 0.04818 kg/s at: a) 735 W/m^2 and b) 935 W/m^2. Entropy generation rate due to: Sv = Viscous effects. Sh = Heat transfer. Sq = Heat loss. Stotal = Total Entropy generation rate.

For the highest solar radiation value (Fig. 12b), the entropy generation rate attributed to heat transfer (S_h) presents global values of 0.15 W/K, 0.04 W/K and 0.035 W/K for pure water, TiO_2 nanofluid and SiO_2 nanofluid respectively. This represents a decrease of 74.5 % between purified water and TiO_2 nanofluid and 77 % between purified water and SiO_2 nanofluid. The entropy generation rate attributed to heat loss (S_q) has global values of 2.22 W/K, 0.73W/K and 2.93 W/K for pure water, TiO_2 nanofluid and SiO_2 nanofluid respectively. This represents a decrease of 67 % between purified water and TiO_2 nanofluid but an increase of 24 % between purified water and SiO_2 nanofluid. This phenomenon is attributed to the adverse effect on the specific heat of the SiO_2 water-based nanofluid, particularly under high solar radiation conditions.

Across all working fluids and for both solar radiation levels, approximately 95 % of the total entropy generation rate is attributed to heat loss (S_q). Moreover, a consistent pattern in the global entropy generation rate is observed across various inlet mass flow rate values.

Fig. 13 shows the global form of the entropy generation rate for the three working fluids under varying inlet mass flow rates and the solar radiation conditions (735 W/m^2 and 935 W/m^2). The global form of the entropy generation rate accounts for viscous effects, heat transfer, and heat loss.

The data showed that the global form of the entropy generation caused by viscous effects (Fig. 13a) rises with an increase in the mass flow rate and solar radiation value. The pure water has the highest entropy generation rate value ($4.7\ x\ 10^{-5}\ W/K$) followed by the TiO_2 nanofluid ($5\ x\ 10^{-6}\ W/K$) and SiO_2 nanofluid ($2\ x\ 10^{-6}\ W/K$). As previously mentioned, the entropy generation attributed to viscous effects is minimal across all working fluids and under all the examined scenarios due to the low velocities obtained.

The global form of the entropy generation rate attributed to heat transfer (Fig. 13b) exhibits a nearly independent behavior concerning changes in the inlet mass flow rate but not with solar radiation values. With higher solar radiation values, the entropy generation rate attributed to heat transfer also has an increment. Specifically, the pure water has the highest entropy generation rate value ($0.16\ W/K$) followed by the TiO_2 nanofluid ($0.054\ W/K$) and the SiO_2 nanofluid ($0.05\ W/K$).

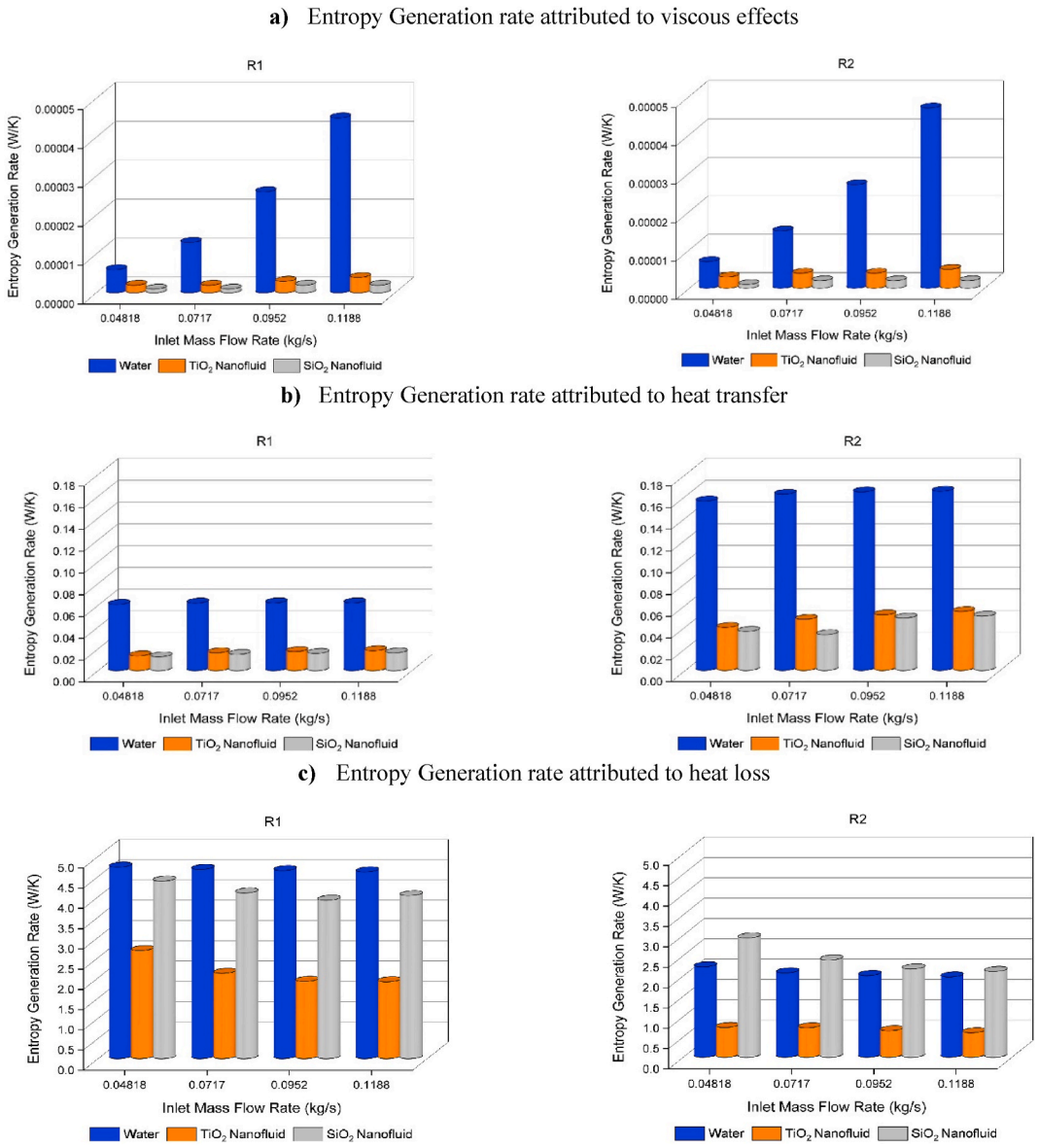

Fig. 13. Global form of the entropy generation rate attributed to a) viscous effects, b) heat transfer and c) heat loss.

The global form of the entropy generation rate attributed to heat loss (Fig. 13c) exhibits a consistent decrease as the inlet mass flow rate increases. Furthermore, the decrease becomes more pronounced with higher solar radiation values. However, at the highest solar radiation value, the SiO_2 nanofluid shows higher entropy generation rate values than pure water as the working fluid. As stated above, there is a negative impact on the specific heat of SiO_2 nanofluid, especially at higher solar radiation values. The pure water at the lowest solar radiation value, has the highest entropy generation rate value (4.7 W/K) followed by the SiO_2 nanofluid (4.4W/K) and TiO_2 nanofluid (1.9 W/K).

In general, using nanofluids reduces the entropy generation rate values, contributing to an improved ETSC performance.

3.6. Local form of the entropy generation rate

Fig. 14 illustrates the local form of the entropy generation rate attributed to viscous effects at both the initial and last tubes of the ETSC. These contours account for the three working fluids under a solar radiation value of 935 W/m^2 and an inlet mass flow rate of 0.04818 kg/s. In the initial tube (Fig. 14a), the entropy generation rate attributed to viscous effects is concentrated in the middle of the manifold for all the working fluids, coinciding with the maximum velocities of the working fluids. In the last tube (Fig. 14b) the entropy generation rate attributed to viscous effects is concentrated at the junction of the manifold and the evacuated tube. Additionally, as the

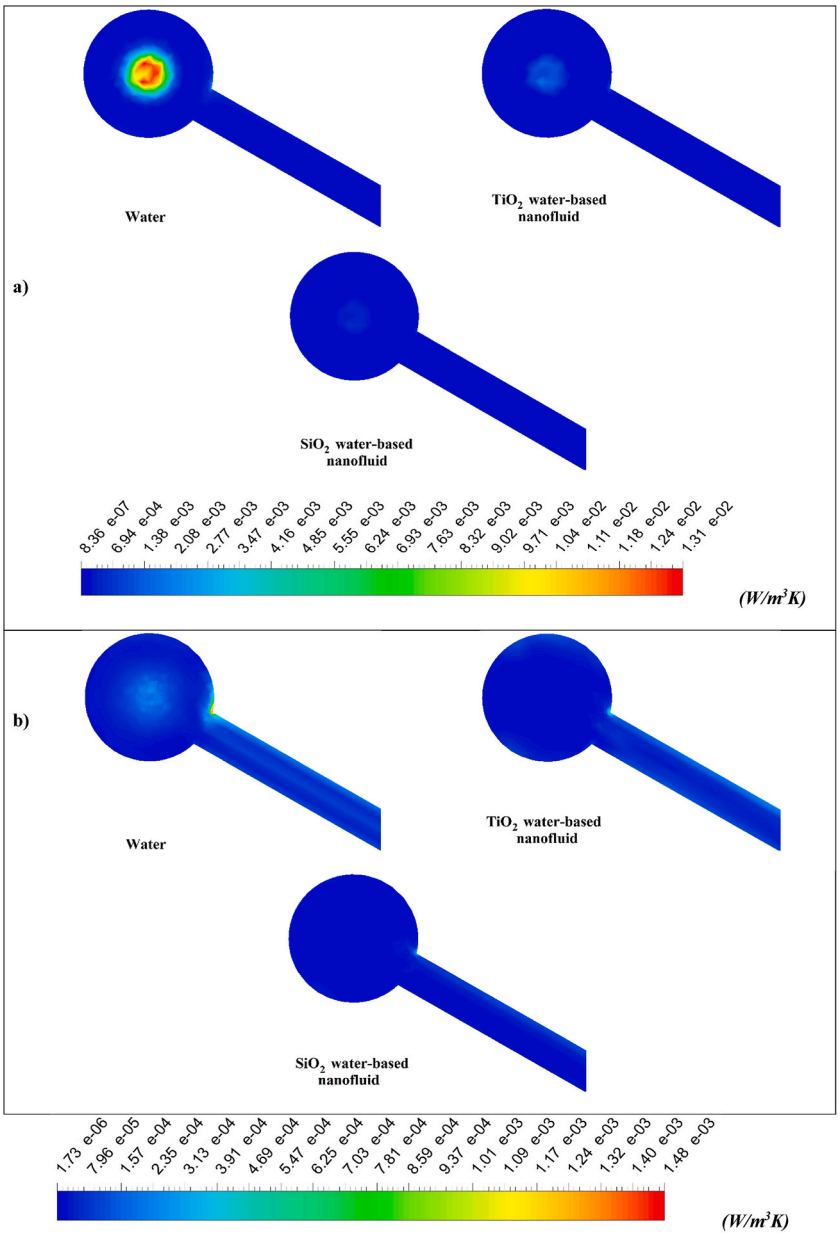

Fig. 14. Local form of the entropy generation rate attributed to viscous effects at the a) initial and b) last tube of the ETSC at 935 W/m^2 (R2) and an inlet mass flow rate of 0.04818 kg/s.

fluid traverses through the ETSC, the entropy generation decreases. The maximum values of the entropy generation attributed to viscous effects are $1.3\,x\,10^{-2}$, $1.6\,x\,10^{-3}$ and $5.3\,x\,10^{-4}\ W/m^3K$ corresponding to pure water, TiO_2 nanofluid and SiO_2 nanofluid respectively. These values are found at the first tube of the ETSC. In general, when nanofluids are employed as working fluids, the local form of the entropy generation attributed to viscous effects is lower.

The contours of the local entropy generation rate attributed to heat transfer, as shown in Fig. 15, are illustrated at both the initial and last tubes of the ETSC. These contours encompass the three working fluids with a solar radiation of 935 W/m^2 and an inlet mass flow rate of 0.04818 kg/s. In the initial tube (Fig. 15a), when using pure water as the working fluid, the concentration of entropy generation rate attributed to heat transfer is observed at the junction of the manifold and the evacuated tube. When nanofluids are utilized, the entropy generation becomes concentrated in the center of the manifold, and this behavior is linked to the temperature gradients inside the ETSC. In the last tube (Fig. 15b) the entropy generation attributed to heat transfer is concentrated at the junction of the manifold and the evacuated tube for all three working fluids. Once again, it is observed that, as the working fluid flows through the ETSC, the entropy generation decreases. The highest local entropy generation rate attributed to heat transfer is recorded at the initial

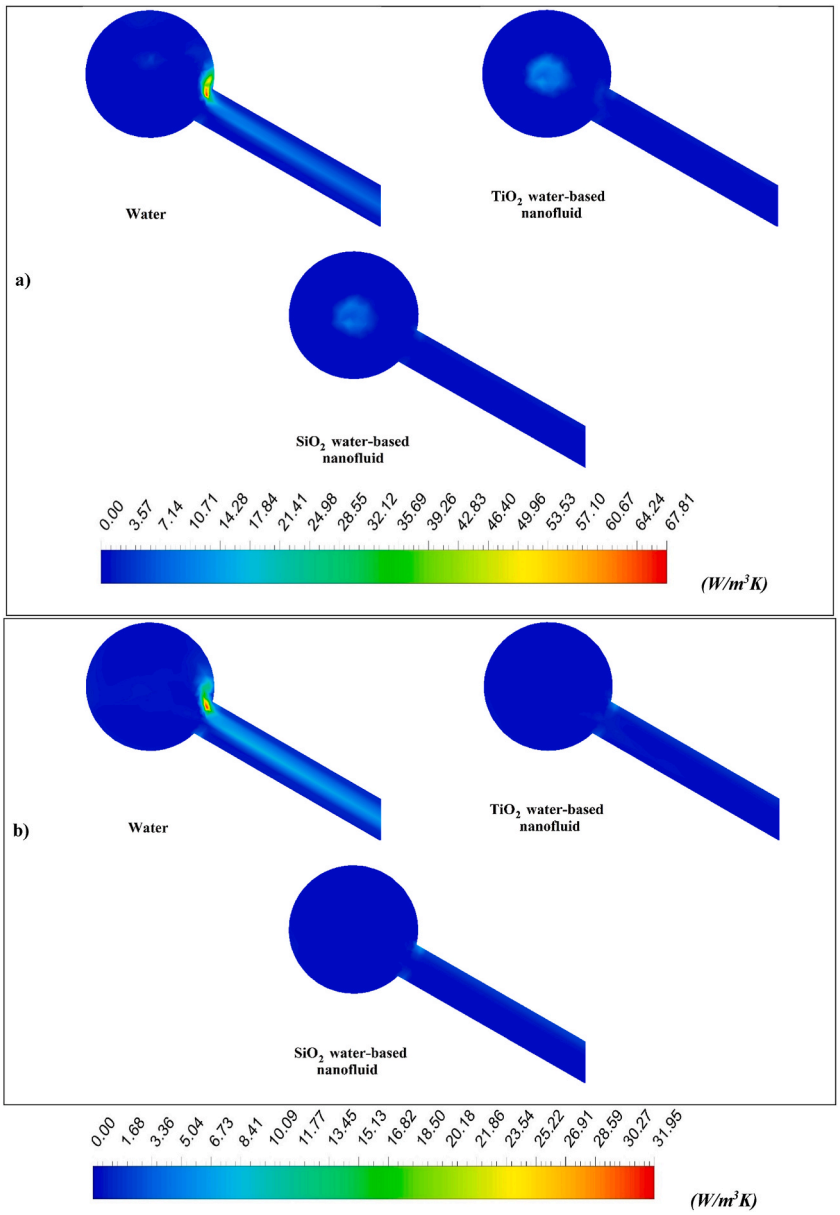

Fig. 15. Local form of the entropy generation rate attributed to heat transfer at the a) initial and b) last tube of the ETSC at 935 W/m^2 (R2) and an inlet mass flow rate of 0.04818 kg/s.

tube of the ETSC, with values of 67.8, 12.8 and 10.4 W/m^3K for pure water, TiO_2 nanofluid and SiO_2 nanofluid respectively. In general, the uniform temperature distribution resulting from the use of nanofluids leads to reduced entropy generation rate attributed to heat transfer.

4. Conclusions

This study provides a comparison of the thermohydraulic performance and entropy generation rate in an evacuated tube solar collector using TiO_2 and SiO_2 nanofluids, as well as pure water, as working fluids. Through 24 simulations conducted via Computational Fluid Dynamics, variations in solar radiation and inlet mass flow rate were explored as operational parameters.

The results demonstrate that TiO_2 nanofluid consistently achieves the highest outlet temperature under all operational conditions, surpassing pure water and SiO_2 nanofluid by 6.8 % and 6.5 %, respectively. Using water-based nanofluids as working fluids results in a more uniform temperature distribution throughout the ETSC, attributing to the modified thermal conductivity of the nanofluids.

While nanofluids result in higher velocities, it is noteworthy that the velocity values remain low for all working fluids. The

combination of alterations in thermal properties, particularly viscosity, thermal conductivity, and density, contributes to the increase in velocity.

The TiO_2 nanofluid consistently shows higher thermal and exergy efficiency 0.86 and 0.022, respectively) across all conditions, aligning with previous findings. However, the SiO_2 nanofluid displays lower efficiency, especially under the highest solar radiation. This is due to SiO_2 nanoparticles' impact on specific heat.

Entropy generation rate attributed to viscous effects remains negligible across all nanofluids, however, the entropy generation rate due to heat transfer increases with solar radiation. On the other hand, the entropy generation rate due to heat loss decreases with higher mass flow rates, particularly with increasing solar radiation. TiO_2 nanofluid shows the lowest entropy generation rate, while SiO_2 nanofluid's specific heat leads to higher entropy generation rate under the highest solar radiation value.

Nanofluid application significantly reduces local entropy generation rate, facilitating the identification of irreversibilities within the ETSC, which are primarily concentrated in the middle of the manifold and at the junction with the evacuated tube.

This study offers valuable insights into the efficiency of an ETSC using different nanofluids, highlighting their potential to enhance performance. In order to promote environmental sustainability, it is recommended to focus on enhancing efficiency and reducing irreversibilities within the ETSC. This could involve further experimentation with different operational parameters, development of innovative design strategies and even different types of nanofluids.

Data availability statement

Data will be made available on request.

CRediT authorship contribution statement

Oscar A. López-Núñez: Writing – review & editing, Writing – original draft, Validation, Supervision, Software, Methodology, Investigation, Formal analysis, Conceptualization. **F. Lara:** Writing – review & editing, Writing – original draft, Validation, Methodology, Investigation, Formal analysis. **A. González-Angeles:** Writing – review & editing, Writing – original draft, Validation, Methodology, Investigation, Formal analysis. **A. Cardenas-Robles:** Writing – review & editing, Writing – original draft, Validation, Methodology, Investigation, Formal analysis. **J.J. Ramírez-Minguela:** Writing – original draft, Validation, Formal analysis. **J. Arturo Alfaro-Ayala:** Writing – original draft, Validation, Formal analysis.

Declaration of competing interest

The authors declare that they have no known competing financial interests or personal relationships that could have appeared to influence the work reported in this paper.

Acknowledgments

The authors express their sincere appreciation to the Consejo Nacional de Humanidades, Ciencias y Tecnologías (CONAHCyT), Mexico, for the financial backing received through the S.N.I.I program and for the financial support of the program "Apoyos Complementarios para Estancias Sabáticas Vinculadas a la Consolidación de Grupos de Investigación 2023".

References

[1] ChM.S. Kumar, S. Singh, M.K. Gupta, Y.M. Nimdeo, R. Raushan, A.V. Deorankar, T.M.A. Kumar, P.K. Rout, C.S. Chanotiya, V.D. Pakhale, A.D. Nannaware, Solar energy: a promising renewable source for meeting energy demand in Indian agriculture applications, Sustain. Energy Technol. Assessments 55 (2023) 102905, https://doi.org/10.1016/j.seta.2022.102905.

[2] M.M. Bhatti, K. Vafai, S.I. Abdelsalam, The role of nanofluids in renewable energy engineering, Nanomaterials 13 (2023) 2671, https://doi.org/10.3390/nano13192671.

[3] M. Murugan, A. Saravanan, P.V. Elumalai, P. Kumar, C. Ahamed Saleel, O.D. Samuel, M. Setiyo, C.C. Enweremadu, A. Afzal, An overview on energy and exergy analysis of solar thermal collectors with passive performance enhancers, Alex. Eng. J. 61 (2022) 8123–8147, https://doi.org/10.1016/j.aej.2022.01.052.

[4] N. Abed, I. Afgan, An extensive review of various technologies for enhancing the thermal and optical performances of parabolic trough collectors, Int. J. Energy Res. 44 (2020) 5117–5164, https://doi.org/10.1002/er.5271.

[5] Q. Xiong, A. Hajjar, B. Alshuraiaan, M. Izadi, S. Altnji, S.A. Shehzad, State-of-the-art review of nanofluids in solar collectors: a review based on the type of the dispersed nanoparticles, J. Clean. Prod. 310 (2021) 127528, https://doi.org/10.1016/j.jclepro.2021.127528.

[6] H. Olfian, S.S.M. Ajarostaghi, M. Ebrahimnataj, Development on evacuated tube solar collectors: a review of the last decade results of using nanofluids, Sol. Energy 211 (2020) 265–282, https://doi.org/10.1016/j.solener.2020.09.056.

[7] S. Ram, S. Kumar Yadav, A. Kumar, Recent advancement of nanofluids in solar concentrating collectors: a brief review, Mater. Today Proc. 72 (2023) 2032–2038, https://doi.org/10.1016/j.matpr.2022.08.078.

[8] M. Mahendran, G.C. Lee, K.V. Sharma, A. Shahrani, Performance of evacuated tube solar collector using water-based titanium oxide nanofluid, J. Mech. Eng. Sci. 3 (2012) 301–310, https://doi.org/10.15282/jmes.3.2012.6.0028.

[9] H. Kim, J. Ham, C. Park, H. Cho, Theoretical investigation of the efficiency of a U-tube solar collector using various nanofluids, Energy 94 (2016) 497–507, https://doi.org/10.1016/j.energy.2015.11.021.

[10] R. Daghigh, P. Zandi, Improving the performance of heat pipe embedded evacuated tube collector with nanofluids and auxiliary gas system, Renew. Energy 134 (2019) 888–901, https://doi.org/10.1016/j.renene.2018.11.090.

[11] E. Elshazly, A. A. Abdel-Rehim, I. El-Mahallawi, Thermal performance enhancement of evacuated tube solar collector using MWCNT, Al2O3, and hybrid MWCNT/Al2O3nanofluids, International Journal of Thermofluids 17 (2023) 100260, https://doi.org/10.1016/j.ijft.2022.100260.

[12] S.M.S. Hosseini, M. Shafiey Dehaj, Assessment of TiO2 water-based nanofluids with two distinct morphologies in a U type evacuated tube solar collector, Appl. Therm. Eng. 182 (2021), https://doi.org/10.1016/j.applthermaleng.2020.116086.

[13] S.B. Sasikumar, H. Santhanam, M.M. Noor, M. Devasenan, H.M. Ali, Experimental investigation of parallel type -evacuated tube solar collector using nanofluids, Energy Sources, Part A Recovery, Util. Environ. Eff. (2020) 1–13, https://doi.org/10.1080/15567036.2020.1829201.

[14] S. Yan, F. Wang, Z.G. Shi, R. Tian, Heat transfer property of SiO2/water nanofluid flow inside solar collector vacuum tubes, Appl. Therm. Eng. 118 (2017) 385–391, https://doi.org/10.1016/j.applthermaleng.2017.02.108.

[15] M. Mercan, A. Yurddaş, Numerical analysis of evacuated tube solar collectors using nanofluids, Sol. Energy 191 (2019) 167–179, https://doi.org/10.1016/j.solener.2019.08.074.

[16] A. Yurddaş, Optimization and thermal performance of evacuated tube solar collector with various nanofluids, Int. J. Heat Mass Tran. 152 (2020) 119496, https://doi.org/10.1016/j.ijheatmasstransfer.2020.119496.

[17] H.A. Hasan, J.S. Sherza, A.M. Abed, H.S. Sultan, K. Sopian, Improve the performance of solar thermal collectors by varying the concentration and nanoparticles diameter of silicon dioxide, Open Eng. 12 (2022) 743–751, https://doi.org/10.1515/eng-2022-0339.

[18] S. Mojtaba Tabarhoseini, M. Sheikholeslami, Modeling of evacuated tube solar collector involving longitudinal fins and nanofluids, Sustain. Energy Technol. Assessments 53 (2022) 102587, https://doi.org/10.1016/j.seta.2022.102587.

[19] O. Mahian, A. Kianifar, C. Kleinstreuer, M.A. Al-Nimr, I. Pop, A.Z. Sahin, S. Wongwises, A review of entropy generation in nanofluid flow, Int. J. Heat Mass Tran. 65 (2013) 514–532, https://doi.org/10.1016/j.ijheatmasstransfer.2013.06.010.

[20] A. Sciacovelli, V. Verda, E. Sciubba, Entropy generation analysis as a design tool—a review, Renew. Sustain. Energy Rev. 43 (2015) 1167–1181, https://doi.org/10.1016/j.rser.2014.11.104.

[21] Y.Y. Gan, H.C. Ong, T.C. Ling, N.W.M. Zulkifli, C.T. Wang, Y.C. Yang, Thermal conductivity optimization and entropy generation analysis of titanium dioxide nanofluid in evacuated tube solar collector, Appl. Therm. Eng. 145 (2018) 155–164, https://doi.org/10.1016/j.applthermaleng.2018.09.012.

[22] S. Kumar, A.K. Tiwari, Performance evaluation of evacuated tube solar collector using boron nitride nanofluid, Sustain. Energy Technol. Assessments 53 (2022) 102466, https://doi.org/10.1016/j.seta.2022.102466.

[23] S.M. Tabarhoseini, M. Sheikholeslami, Entropy generation and thermal analysis of nanofluid flow inside the evacuated tube solar collector, Sci. Rep. 12 (2022), https://doi.org/10.1038/s41598-022-05263-2.

[24] P. Naphon, S. Wiriyasart, Pulsating flow and magnetic field effects on the convective heat transfer of TiO2-water nanofluids in helically corrugated tube, Int. J. Heat Mass Tran. 125 (2018) 1054–1060, https://doi.org/10.1016/j.ijheatmasstransfer.2018.05.015.

[25] R.K. Ajeel, W.S.-I. Salim, K. Sopian, M.Z. Yusoff, K. Hasnan, A. Ibrahim, A.H.A. Al-Waeli, Turbulent convective heat transfer of silica oxide nanofluid through corrugated channels: an experimental and numerical study, Int. J. Heat Mass Tran. 145 (2019) 118806, https://doi.org/10.1016/j.ijheatmasstransfer.2019.118806.

[26] J.J. Ramírez-Minguela, J.A. Alfaro-Ayala, V.H. Rangel-Hernández, A.R. Uribe-Ramírez, J.M. Mendoza-Miranda, V. Pérez-García, J.M. Belman-Flores, Comparison of the thermo-hydraulic performance and the entropy generation rate for two types of low temperature solar collectors using CFD, Sol. Energy 166 (2018) 123–137, https://doi.org/10.1016/j.solener.2018.03.050.

[27] C.S.L. Lim, S. Sobhansarbandi, CFD modeling of an evacuated U-tube solar collector integrated with a novel heat transfer fluid, Sustain. Energy Technol. Assessments 52 (2022) 102051, https://doi.org/10.1016/j.seta.2022.102051.

[28] M. Karami, N. Shahini, M. Ali Akhavan Behabadi, Numerical investigation of double-walled direct absorption evacuated tube solar collector using microencapsulated PCM and nanofluid, J. Mol. Liq. 377 (2023) 121560, https://doi.org/10.1016/j.molliq.2023.121560.

[29] M. Singla, V.S. Hans, S. Singh, CFD analysis of rib roughened solar evacuated tube collector for air heating, Renew. Energy 183 (2022) 78–89, https://doi.org/10.1016/j.renene.2021.10.055.

[30] M. Abrofarakh, H. Moghadam, Investigation of thermal performance and entropy generation rate of evacuated tube collector solar air heater with inserted baffles and metal foam: a CFD approach, Renew. Energy 223 (2024) 120022, https://doi.org/10.1016/j.renene.2024.120022.

[31] O.A. López-Núñez, J. Arturo Alfaro-Ayala, J.J. Ramírez-Minguela, J. Nicolás Flores-Balderas, J.M. Belman-Flores, Solar radiation model applied to a low temperature evacuated tubes solar collector, J. Sol. Energy Eng. 141 (2018) 031003, https://doi.org/10.1115/1.4041402.

[32] Z. Said, M. Iqbal, A. Mehmood, T.T. Le, H.M. Ali, D.N. Cao, P.Q.P. Nguyen, N.D.K. Pham, Nanofluids-based solar collectors as sustainable energy technology towards net-zero goal: recent advances, environmental impact, challenges, and perspectives, Chemical Engineering and Processing - Process Intensification 191 (2023) 109477, https://doi.org/10.1016/j.cep.2023.109477.

[33] Y. Wenceslas Koholé, F. Cyrille Vincelas Fohagui, G. Tchuen, Flat-plate solar collector thermal performance assessment via energy, exergy and irreversibility analysis, Energy Convers. Manag. X 15 (2022) 100247, https://doi.org/10.1016/j.ecmx.2022.100247.

[34] M. Eltaweel, A.A. Abdel-Rehim, A.A.A. Attia, A comparison between flat-plate and evacuated tube solar collectors in terms of energy and exergy analysis by using nanofluid, Appl. Therm. Eng. 186 (2021) 116516, https://doi.org/10.1016/j.applthermaleng.2020.116516.

[35] A. Veera Kumar, T.V. Arjunan, D. Seenivasan, R. Venkatramanan, S. Vijayan, M.M. Matheswaran, Influence of twisted tape inserts on energy and exergy performance of an evacuated Tube-based solar air collector, Sol. Energy 225 (2021) 892–904, https://doi.org/10.1016/j.solener.2021.07.074.

[36] S. Kumar Priyanka, A. Kumar, R. Maithani, S. Sharma, D. Singh, Exergy analysis of various solar thermal collectors, Mater. Today Proc. (2022), https://doi.org/10.1016/j.matpr.2022.08.543.

[37] J.A. Alfaro-Ayala, O.A. López-Núñez, F.I. Gómez-Castro, J.J. Ramírez-Minguela, A.R. Uribe-Ramírez, J.M. Belman-Flores, S. Cano-Andrade, Optimization of a solar collector with evacuated tubes using the simulated annealing and computational fluid dynamics, Energy Convers. Manag. 166 (2018) 343–355, https://doi.org/10.1016/j.enconman.2018.04.039.

[38] Z. Said, R. Saidur, A. Hepbasli, N.A. Rahim, New thermophysical properties of water based TiO2 nanofluid-The hysteresis phenomenon revisited, Int. Commun. Heat Mass Tran. 58 (2014) 85–95, https://doi.org/10.1016/j.icheatmasstransfer.2014.08.034.

[39] S. Etaig, R. Hasan, N. Perera, Investigation of a new effective viscosity model for nanofluids, in: Procedia Eng, Elsevier Ltd, 2016, pp. 404–413, https://doi.org/10.1016/j.proeng.2016.08.383.

[40] F. Rubbi, L. Das, K. Habib, N. Aslfattahi, R. Saidur, M.T. Rahman, State-of-the-art review on water-based nanofluids for low temperature solar thermal collector application, Sol. Energy Mater. Sol. Cell. 230 (2021), https://doi.org/10.1016/j.solmat.2021.111220.

[41] S. Mukherjee, S. Chakrabarty, P.C. Mishra, P. Chaudhuri, Transient heat transfer characteristics and process intensification with Al2O3-water and TiO2-water nanofluids: an experimental investigation, Chemical Engineering and Processing - Process Intensification 150 (2020), https://doi.org/10.1016/j.cep.2020.107887.

[42] T.K. Murtadha, Effect of using Al2O3/TiO2 hybrid nanofluids on improving the photovoltaic performance, Case Stud. Therm. Eng. 47 (2023) 103112, https://doi.org/10.1016/j.csite.2023.103112.

[43] M.M. Sorour, W.M. El-Maghlany, M.A. Alnakeeb, A.M. Abbass, Experimental study of free single jet impingement utilizing high concentration SiO nanoparticles water base nanofluid, Appl. Therm. Eng. 160 (2019) 114019, https://doi.org/10.1016/j.applthermaleng.2019.114019.

[44] O.A. López-Núñez, J.A. Alfaro-Ayala, J.J. Ramírez-Minguela, F. Cano-Banda, B. Ruiz-Camacho, J.M. Belman-Flores, Numerical analysis of the thermo-hydraulic performance and entropy generation rate of a water-in-glass evacuated tube solar collector using TiO2 water-based nanofluid and only water as working fluids, Renew. Energy 197 (2022) 953–965, https://doi.org/10.1016/j.renene.2022.07.156.

[45] D. Groot, S. Ruurds, P. Mazur, Non-Equilibrium Thermodynamics, Dover Publications, New York, 2011.

[46] P. Liu, N. Zheng, Z. Liu, W. Liu, Thermal-hydraulic performance and entropy generation analysis of a parabolic trough receiver with conical strip inserts, Energy Convers. Manag. 179 (2019) 30–45, https://doi.org/10.1016/j.enconman.2018.10.057.

[47] H. Kaya, M. Alkasem, K. Arslan, Effect of nanoparticle shape of Al2O3/Pure Water nanofluid on evacuated U-Tube solar collector efficiency, Renew. Energy 162 (2020) 267–284, https://doi.org/10.1016/j.renene.2020.08.039.

[48] J.J. Ramírez-Minguela, V.H. Rangel-Hernández, J.A. Alfaro-Ayala, F. Elizalde-Blancas, B. Ruiz-Camacho, O.A. López-Núñez, C.E. Alvarado-Rodríguez, Performance comparison of different flat plate solar collectors by means of the entropy generation rate using computational fluid dynamics, Entropy 25 (2023) 621, https://doi.org/10.3390/e25040621.
[49] J.R. Satti, D.K. Das, D.R. Ray, Measurements of densities of propylene glycol-based nanofluids and comparison with theory, J. Therm. Sci. Eng. Appl. 8 (2016), https://doi.org/10.1115/1.4032671.
[50] Z. Said, R. Saidur, Thermophysical properties of metal oxides nanofluids, in: Nanofluid Heat and Mass Transfer in Engineering Problems, InTech, 2017, https://doi.org/10.5772/65610.
[51] M. Rejvani, A. Alipour, S.M. Vahedi, A.J. Chamkha, S. Wongwises, Optimal characteristics and heat transfer efficiency of SiO2/water nanofluid for application of energy devices: a comprehensive study, Int. J. Energy Res. (2019), https://doi.org/10.1002/er.4854 er.4854.
[52] X. Xia, X. Cao, N. Li, B. Yu, H. Liu, Jie ji, Study on a spectral splitting photovoltaic/thermal system based on CNT/Ag mixed nanofluids, Energy 271 (2023) 127093, https://doi.org/10.1016/j.energy.2023.127093.
[53] J.A. Alfaro-ayala, G. Martínez-rodríguez, M. Picón-núñez, A.R. Uribe-ramírez, A. Gallegos-muñoz, Numerical study of a low temperature water-in-glass evacuated tube solar collector, Energy Convers. Manag. 94 (2015) 472–481.
[54] S. Mondal, S.K. Majumder, Heat transport based on hydrodynamics and the local entropy generation rate in straight and serpentine rectangular packed narrow channels, Appl. Therm. Eng. 171 (2020) 115057, https://doi.org/10.1016/j.applthermaleng.2020.115057.
[55] Z. Said, M. Ghodbane, B. Boumeddane, A.K. Tiwari, L.S. Sundar, C. Li, N. Aslfattahi, E. Bellos, Energy, exergy, economic and environmental (4E) analysis of a parabolic trough solar collector using MXene based silicone oil nanofluids, Sol. Energy Mater. Sol. Cell. 239 (2022) 111633, https://doi.org/10.1016/j.solmat.2022.111633.
[56] S. Ataee, M. Ameri, Energy and exergy parameter analysis of a U-pipe evacuated tubular solar collector with filled and unfilled layer, Appl. Therm. Eng. 233 (2023) 121190, https://doi.org/10.1016/j.applthermaleng.2023.121190.
[57] A.D. Tuncer, İ. Aytaç, H.İ. Variyenli, A. Khanlari, S. Mantıcı, A. Karartı, Improving the performance of a heat pipe evacuated solar water collector using a magnetic NiFe2O4/water nanofluid, Therm. Sci. Eng. Prog. 45 (2023) 102107, https://doi.org/10.1016/j.tsep.2023.102107.